

# Silica encapsulation and magnetic properties of FePt nanoparticles

M. Aslam, L. Fu, S. Li, Vinayak P. Dravid\*

*Department of Materials Science and Engineering, and Institute for Nanotechnology, Northwestern University, Evanston, IL 60208, USA*

Received 8 January 2005; accepted 14 April 2005

Available online 2 June 2005

## Abstract

Core-shell nanoparticles have emerged as an important class of functional nanostructures with potential applications in many diverse fields, especially in health sciences. We have used a modified aqueous sol-gel route for the synthesis of size-selective FePt@SiO<sub>2</sub> core-shell nanoparticles. In this approach, oleic acid and oleyl amine stabilized FePt nanoparticles are first encapsulated through an aminopropoxysilane (APS) monolayer and then subsequent condensation of triethoxysilane (TEOS) on FePt particle surface. These well-defined FePt@SiO<sub>2</sub> core-shell nanoparticles with narrow size distribution become colloidal in aqueous media, and can thus be used as carrier fluid for biomolecular complexes. In comparison, the scarce hydrophilic nature of oleic acid monolayers on FePt particle surface yields an edgy partial coating of silica when only TEOS is applied for the surface modification. The synthesized core-shell nanoparticles were characterized by direct techniques of high resolution transmission electron microscopy (HRTEM), EDS and indirectly via UV-vis absorption and FTIR studies. The FePt@SiO<sub>2</sub> nanoparticles exhibit essential characteristics of superparamagnetic behavior, as investigated by SQUID magnetometry. The blocking temperatures ( $T_B$ ) of FePt and FePt@SiO<sub>2</sub> (135 and 80 K) were studied using zero field cooled (ZFC)/field cooled (FC) curves. © 2005 Elsevier Inc. All rights reserved.

**Keywords:** FePt nanoparticles; Silica; Core-shell; Sol-gel; Colloids

## 1. Introduction

The recent thrust to synthesize functional nanoscale particles stems from their fundamental and technological importance [1–4]. Nanoscale materials exhibit interesting electrical, optical, and magnetic properties which are often distinct from their bulk counterparts. Among these, magnetic nanoparticles with size range of 2–10 nm are of particular significance because of their potential applications in multiterabit magnetic storage devices and as carriers for biochemical complexes, MRI contrast enhancing agents, among many other applications [5]. These nanoparticles could also be used as ferrofluids, magnetic refrigeration systems, magnetic resonance imaging, magnetic carriers for drug targeting and catalysis [6,7]. However, some materials such as Co, Ni-based can be biohazardous and also prone toward easy

oxidation or degradation at ambient conditions, hence an increased interest in coating their surface with a thin protecting shell for various biomedical applications. Current methods use micrometer-sized magnetic-polymer/silica particles which are too large for in vivo applications [8]. Recently, less than 20 nm size has been suggested for efficient diffusion of nanoparticles through tissues in MRI imaging [9]. Thus, developing nanometer scale encapsulated magnetic nanoparticles and the investigation of their properties are assuming greater importance.

Most of the work in the past has been on noble-metal nanocores and molecular shells, and monolayers anchored on metal cores have been used as precursors to make oxide shells [4,10]. An approach in this direction is to coat gold clusters with silica shell [10]. We have used an analogous approach to coat the magnetic FePt nanoparticles with silica shells, and focus the synthesis and characterization of colloidal and redispersable FePt@SiO<sub>2</sub> nanoparticles. The coating prevents the aggregation in liquid, has better chemical stability as compared to their bare counterparts and

\* Corresponding author.

E-mail address: [v-dravid@northwestern.edu](mailto:v-dravid@northwestern.edu) (V.P. Dravid).

provides a biofunctional surface for modification and subsequent DNA/protein attachment.

In the recent past, various researchers have suggested encapsulation of magnetite and other ferrite materials [11,12]; however, the literature for the effective surface functionalization of metallic nanoparticles like FePt, Co, and Fe etc. is very sparse [13]. These metallic nanoparticles have higher performance because of their much higher susceptibility and saturation magnetization as compared to magnetite or ferrites. We have initiated this work on oxide protection of metallic/magnetic nanoparticles because this is a way to stabilize these particles under any extreme condition. This type of encapsulation also makes it possible to modify the surface of silica for bimolecular attachment, which can deliver specific ligands to target sites via the antibody–antigen recognition. Also, magnetic nanoparticles have fueled both fundamental and applied studies due to their magnetic properties (e.g., large uniaxial magnetocrystalline anisotropy,  $K_u \cong 7 \times 10^6 \text{ J/m}^3$ ) and enhanced stability [13].

This is the first report where we elucidate the homogeneous and uniform encapsulation of monodispersed FePt nanoparticles with controlled thickness of silica. Since surface functionalization plays an important role in many biological systems, such type of core–shell structures are key in designing complicated multilayer structures with promising applications in biomolecular therapeutics. We use high resolution electron microscopy (HRTEM), UV–vis spectroscopy, infrared spectroscopy (FTIR), and magnetic measurements (SQUID) as the characterization tools to reveal the core–shell structure formation in magnetic nanoparticles.

## 2. Experimental

The FePt nanoparticles synthesis was carried out using standard airless procedures and commercially available reagents [5]. Phenyl ether (99%), 1,2-hexadecanediol (90%), oleic acid (90%), iron pentacarbonyl ( $\text{Fe}(\text{CO})_5$ ), oleylamine (70%), and platinum acetylacetonate ( $\text{Pt}(\text{acac})_2$ ) were purchased from Aldrich Chemical Co.

A typical synthesis route is as follows: 0.5 mM  $\text{Pt}(\text{acac})_2$  and 1.5 mM hexadecanediol were mixed in 20 ml diethyl ether and heated up to 110 °C. Equal amount (1 mM) of oleic acid and oleyl amine were then added with  $\text{Fe}(\text{CO})_5$  and this mixture was heated up to 300 °C for 1 h. The reaction was carried out under  $\text{N}_2$  atmosphere. The black colored solution was allowed to cool to room temperature and precipitated by adding excess ethanol. The magnetic particles were separated using a strong magnet. Dark-yellow supernatant was discarded. After washing several times with ethanol, the precipitate was uniformly dispersed in hexane with small amount of surfactants.

Further, these FePt nanoparticles were encapsulated using two different sol–gel processes. A 0.5 ml hexane based FePt solution was added in 20 ml ethanol containing 0.1 ml triethoxysilane (TEOS). Under continuous mechanical stir-

ring, 1 ml  $\text{NH}_4\text{OH}$  solution (30%) was added slowly to this rigorously stirred mixture. After 3 h, the encapsulated particles were separated using magnet and the excess silica formed during the hydrolysis–condensation was washed off using extensive ethanol washing [11a]. In comparison to direct TEOS condensation, in yet another process the FePt particles with a mean size of  $\sim 5.5$  nm in hexane were mixed with 1 mM APS and the suspension was left for 2 h for place exchange with oleic amine monolayers [11b]. APS monolayers are covalently attached onto the surface of nanoparticles. The APS modified nanoparticles are then used as a source of nucleation of TEOS condensation. A strong magnet was used to separate these APS monolayer covered particles and the particles were subsequently suspended in 100 ml ethanol containing 14  $\mu\text{l}$  TEOS. The solution was stirred continuously while adding 10 ml deionized water for the hydrolysis of TEOS. The final solution was stirred 3 h. The particles were collected with a magnet and repeatedly washed with ethanol. This approach provides great flexibility in the selection of magnetic core. Consequently, magnetic tunability is able to be introduced into these core–shell nanoparticulate systems to achieve the desired superparamagnetic response.

High resolution electron microscopy (HRTEM) measurements were performed on FePt and FePt@ $\text{SiO}_2$  samples which were drop-casted onto a carbon-coated Au grid (Hitachi HF-2000 TEM, Japan). Elemental analysis was performed using EDS system attached to the same instrument. FTIR spectra were acquired with a Bio-Rad Win-IR spectrometer with a resolution of  $2 \text{ cm}^{-1}$ . The samples were prepared by dropcasting the particle solutions in hexane and alcohol (FePt@ $\text{SiO}_2$ ) onto a KBr plate to form a thick film, and further dried in a gentle  $\text{N}_2$  stream. UV–vis spectroscopy was carried out with an UV–vis Czerny–Turner double beam spectrometer with a 1-cm quartz cuvette. Solutions were prepared typically at a concentration of 0.1 mg/ml in hexane and water respectively for FePt and FePt@ $\text{SiO}_2$  particles. Magnetic measurements of FePt and FePt@ $\text{SiO}_2$  were done using SQUID analyzer (Quantum Design, MPMS). The magnetization was measured from room temperature to low temperature. Hysteresis was measured at room temperature. Blocking temperature ( $T_B$ ) was measured using ZFC and FC measurements with  $M$  vs  $T$  curve at an external magnetic field of 500 Oe.

## 3. Results and discussion

We first focused our attention to synthesize uniformly distributed FePt nanoparticles using the route which Sun et al. [5] have reported earlier. While they used size-selective precipitation to obtain monodispersion (std. deviation  $\sim 10\%$ ), we acquired a fairly uniform distribution by controlled addition of a reducing agent. These particles are stabilized using a small amount of oleic acid and oleyl amine in hexane. Fig. 1A shows the TEM image of uniform distri-

bution of FePt nanoparticles which are surface protected by oleic acid and oleyl amine. The particles have a narrow size distribution with an average size of  $5.0 \pm 0.5$  nm. High resolution TEM studies (Fig. 1A inset) indicate the crystalline nature of these nanoparticles. These particles are expected to be a single magnetic domain and exhibit magnetic moment

only in the presence of magnetic field indicating superparamagnetic nature. When magnetic field is removed, the particles return to their nonmagnetic state immediately.

Figs. 1B and 1C show the two typical core-shell TEM images of FePt@SiO<sub>2</sub> nanoparticles with the darker region in the centre for Fig. 1C probably due to the homogeneous

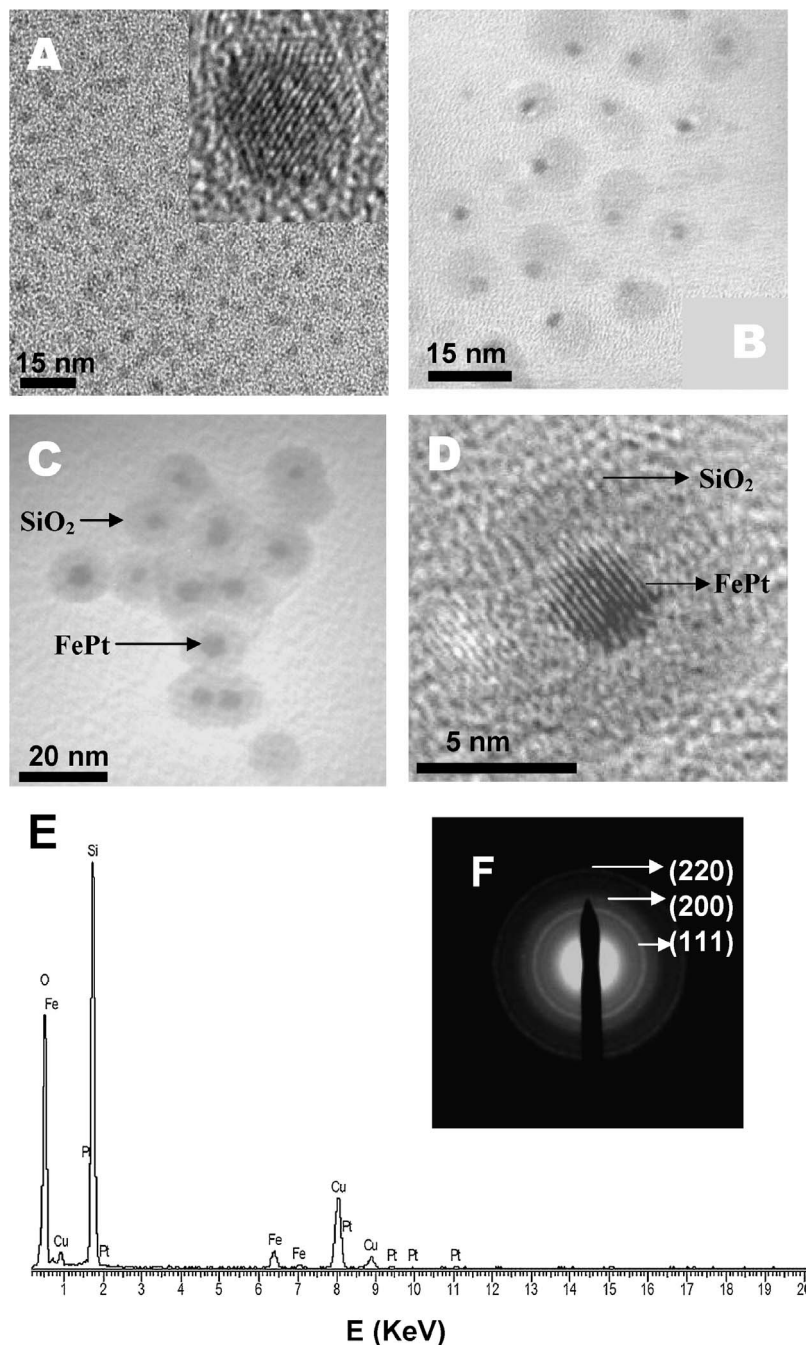


Fig. 1. (A) TEM image of the oleic acid and oleyl amine surface protected FePt nanoparticles. The film was drop-casted by putting a drop of hexane-dispersed FePt nanoparticles on carbon-coated copper grid. Inset shows the lattice imaging of a single FePt nanoparticle. (B) Low magnification TEM image of FePt nanoparticles whose surface is scarcely protected by insulating SiO<sub>2</sub> shell. Direct TEOS hydrolysis–condensation method was used here for the shell formation. (C) Low resolution TEM image of few FePt@SiO<sub>2</sub> nanoparticles indicating uniform coating of silica. APS:TEOS monolayer and then condensation method was applied here. (D) A HRTEM image of the FePt@SiO<sub>2</sub> nanoparticle indicating the amorphous nature of the silica shell which is  $\sim 3$  nm in thickness. (E) EDS of silica portion of a FePt@SiO<sub>2</sub> nanoparticles when the beam was focused on silica edges. (F) Select area electron diffraction pattern of the FePt nanocrystals recorded by focusing the beam on individual nanoparticle.

growth of silica on APS place-exchanged monolayers on top of the particles before the TEOS hydrolysis and condensation. In comparison, a direct growth of silica using only pure TEOS condensation pushing the shell on a side of particles surface might be due to scarce hydrophilicity provided by the oleic acid and oleic amine monolayers. The central dark region is 5 nm FePt and the lighter ring is 10–12 nm silica shell (Fig. 1B) and 4 nm (Fig. 1C). The different contrast between the core and shell region is due to the different electron penetration efficiency on metallic FePt and oxide silica. Detailed structure of a single FePt@SiO<sub>2</sub> particle is characterized with HRTEM, as shown in Fig. 1D. The lattice fringes of the core are clearly shown in the image with adjacent fringe spacing of 0.224 nm corresponding to {111} lattice planes for FePt.

Because XRD of nanoparticles leads to considerable broadening of the diffraction peaks, we have relied on electron diffraction to confirm the crystallinity and crystal structure of these nanoparticles. HRTEM in combination with selected area electron diffraction (SAED) analysis reveals that the structure of the core is consistent with chemically disordered FCC (Fig. 1F) alloy. Individual electron diffraction spots of Fe and Pt are not present while X-ray microanalysis showed presence of Pt and Fe (and Si from shells). Additionally, the uniform lattice fringes across the particles from HRTEM image demonstrate that the particles are homogeneous. The *d*-spacings measured from the patterns and the relative intensities of the diffraction spots are consistent with metallic FePt. EDS analyses of the core/shell nanoparticles reveal that the average composition of these particles is Fe/Pt = 76:24, a ratio larger than the one at 58:42 earlier reported in the literature [5]. The variation in FePt composition as compared to the reported value may be due to the lack of reduction of Fe salt in a polyol process. The redox potential of the reducing agent may have a more negative value than that of the metal species. A stronger reducing agent is needed for the reduction of more electronegative metal and Pt is known to play a critical role in inducing and accelerating the reduction of associated metal cation [14]. Although the species are reduced at comparatively low rate, the FCC structure is still maintained, which suggests that the standard reduction potential difference for Fe<sup>2+</sup>/Fe and Pt<sup>2+</sup>/Pt plays a key role in this synthesis. Clearly, however, the reaction mechanism needs to be more carefully investigated to understand the nucleation and growth process of the particles and for process control. The Si and O peaks are more pronounced after concentrating the electron beam on the shell portion of the silica-coated FePt particles (Fig. 1E). High resolution TEM studies show that the amorphous shells completely cover the magnetic crystalline particles (Fig. 1D) rendering them aqueous stable and hence a useful platform for biofunctionalization.

Fig. 2 shows the UV–vis spectra of FePt in hexane and FePt@SiO<sub>2</sub> in water. The absorption at 273 nm originates from the FePt parts, which agrees with the spectra of previous observations [15], and the peak at ~205 nm likely

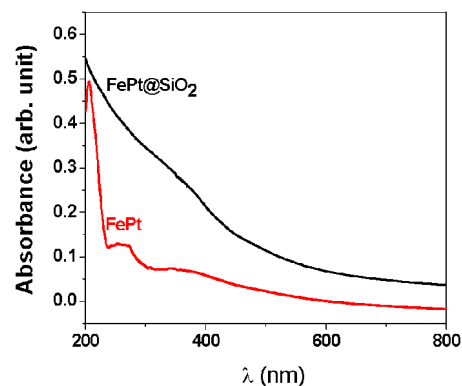


Fig. 2. UV–vis spectra of FePt and FePt@SiO<sub>2</sub> nanoparticles in hexane and aqueous conditions, respectively.

originates from the surfactant. The addition of silica layer is marked by a pronounced scattering and broadening of the absorption peak and the FePt absorption peak disappears for the FePt@SiO<sub>2</sub> colloids. Obviously, the surface plasmon band of alloy particles is screened by the strong scattering from the silica colloid. These results can be corroborated visually by the loss of the characteristic dark brown color to a pale yellow colored solution with fine colloidal dispersion after silica adsorption on FePt surface. This observation is indicative of colloidal stability which is essential for further biological targeting.

FTIR spectroscopy has been used previously to examine the conformational structure of the particle-bound organic surfactant monolayers, where the energies of the symmetric (*d*<sup>+</sup>) and antisymmetric (*d*<sup>-</sup>) stretching vibrations of the methylene units are taken as a sensitive diagnostic indicator for the ordering of the adsorbed organic molecules. Despite the rapid advances made in characterizing these interesting materials, we were interested to understand the structure and orientation of oleic acid and oleic amine molecules after the silica shell formation on functionalized FePt particles, and possible losses, if any, during their ‘pull’ in aqueous condition. Using drop-cast thick films of the above-obtained FePt particles, the FTIR spectra for the samples show bands corresponding to methylene symmetric and asymmetric stretches at 2848.5 and 2914 cm<sup>-1</sup>, corresponding to the hydrocarbon chain of oleic acid and oleic amine, indicating that the hydrocarbon chains surrounding the nanoparticles are highly ordered in the solid state (Fig. 3A). In comparison, in pure oleic acid and oleic amine and mixture of both [16], the two vibrational modes are found at 2922 and 2854 cm<sup>-1</sup>, whereas in liquid heptylamine they arise at 2926 and 2855 cm<sup>-1</sup>. Thus, one can see that the FePt particle-bound amine and carboxylate monolayers resemble the crystalline state, presumably with low density of defects which indicates high surface density of these molecules is promoting the ordering. In comparison, the silica shell on the surface locks the methylene vibration significantly and the symmetric (*d*<sup>+</sup>) band shifts to higher wavenumber (2879.75 cm<sup>-1</sup>) while the antisymmetric (*d*<sup>-</sup>) band remains at the same position (2914 cm<sup>-1</sup>). While the

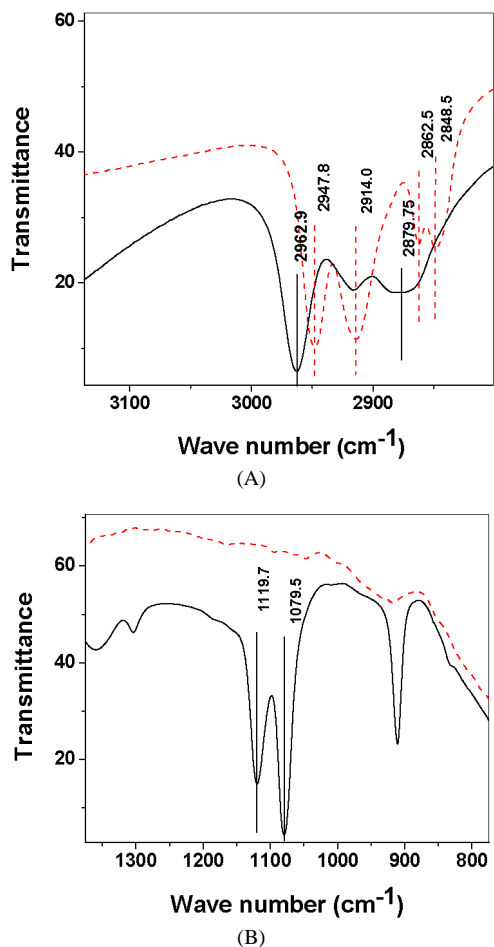


Fig. 3. The FTIR spectra recorded from a drop-casted FePt (---) and FePt@SiO<sub>2</sub> (—) nanoparticles on a KBr disc: (A) in the range of 2700–3200 cm<sup>-1</sup> and (B) in the range of 750–1400 cm<sup>-1</sup>. The main resonances are identified in the figure and discussed in the text with reference to *n*-alkane and Si–O vibrations on solid surfaces.

reason for this unidirectional shift is not clear at the moment, we speculate it may be due to the coordination of the some of the –OH functional groups from the silica growth. The presence of silica was mainly confirmed by the vibration spectrum of Si–O–Si at around 1070 ± 10 and 1110 ± 10 cm<sup>-1</sup> that were consistent with a shell of partially and fully condensed siloxane centers (Fig. 3B). In brief, the position and the maintenance in the intensity of the methylene vibrations after silica layer formation indicate the structural integrity of the oleic amine and oleic acid molecules and that solvent entrapment or multilayer formation does not deteriorate the amine and carboxylate monolayers on nanoparticle surface.

Considering the most striking difference evidenced by the structural and morphological characterization of the FePt and FePt@SiO<sub>2</sub> samples in the presence of a thin layer of silica at the surface of the magnetic nanoparticles, the magnetic properties of the powder samples were investigated. Two different procedures to make core–shell structures account for the effect of an additional APS layer and it is believed that the magnetic core size will be affected by the presence of nonmagnetic APS layer on the surface of FePt particles. The

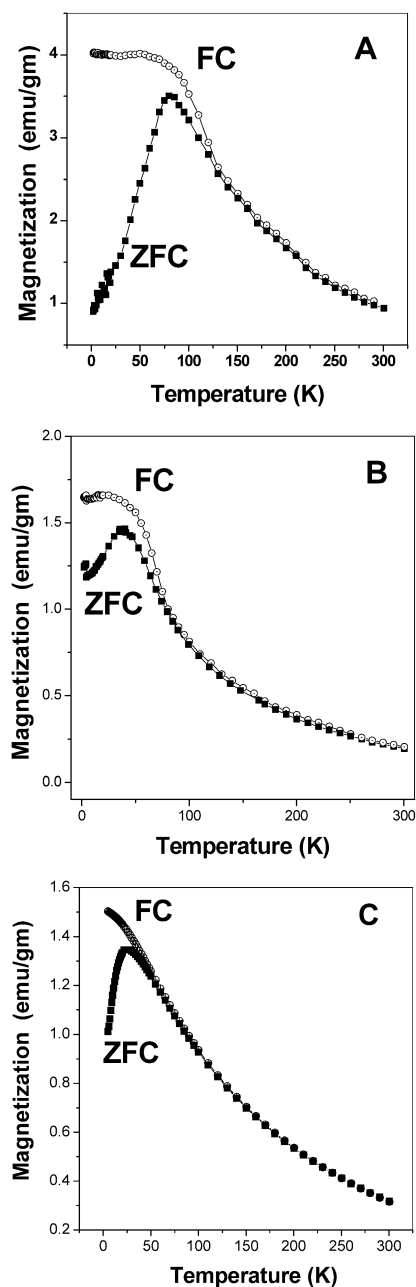


Fig. 4. (A) ZFC/FC curve for FePt (only) nanoparticles. (B) ZFC/FC for FePt@SiO<sub>2</sub> nanoparticles when SiO<sub>2</sub> was grown directly on FePt surface. (C) ZFC/FC curves for FePt@SiO<sub>2</sub> nanoparticles when APS was used as a primer. The field applied for magnetization was 500 Oe.

temperature dependence of magnetization (zero field cooled (ZFC) and field cooled (FC)) measured at the magnetic field of 500 Oe for monodispersed FePt and FePt@SiO<sub>2</sub> (with and without applying APS monolayers as primer on FePt nanoparticles) nanoparticles at the room temperature is shown in Fig. 4. The blocking temperature ( $T_B$ ) is determined by the merge point of ZFC and FC curves. The blocking of FePt nanoparticles is about 140 K (Fig. 4A) and about 90 K (Fig. 4B) for (direct) silica-coated FePt nanoparticles and reduces further down to 60 K when APS is used as an anchor for silica growth. It indicates that silica layer

covers individual FePt nanoparticle, which is consistent with TEM and EDS results. The interparticle separation increases in silica-coated FePt nanoparticles, thus reducing the magnetic dipole–dipole interaction. This leads to a significant shift in  $T_B$  to lower temperature. We believe that an additional APS layer which is also directly affecting the surface states of FePt may further screen the dipolar interaction and the ultimate loss of superparamagnetic fraction. It is interesting to note that these results are in agreement with the theoretical predictions [17] where Monte Carlo simulation was applied to study the decrease in  $T_B$  with decreasing the strength of interaction, but it is not affected by a broader particle size distributions.

#### 4. Conclusions

We have shown that FePt can be encapsulated with insulating and protective silica shell using modified sol–gel routes. We are able to stabilize metallic nanoparticles with oxide shells and make them water dispersible after silica-functionalization. The magnetization behavior of silica-coated FePt nanoparticles indicates a diamagnetic contribution from the shell to the net magnetization of the FePt nanoparticles. The method presented in this paper has been used in making other transition-metal-containing core–shell nanoparticles like Co, Fe, Ni@SiO<sub>2</sub> and these results will be reported later. We believe that successful synthesis of core–shell magnetic structures have potential applications where surface functionalities of SiO<sub>x</sub> shell can be invoked, especially in biomedical field.

#### Acknowledgments

This research is supported by AFOSR-MURI, NSF-NSEC, and NU-IBNAM. Discussions about FTIR spectra with Dr. Mukti Rao (NU, Chemistry Department) are gratefully acknowledged.

#### References

- [1] J.S. Bradley, in: G. Schmid (Ed.), *Clusters and Colloids*, VCH, New York, 1994.
- [2] C.B. Murray, C.R. Kagan, M.G. Bawendi, *Science* 287 (2000) 1989.
- [3] (a) A.P. Alivisatos, *Science* 271 (1996) 933;  
(b) F. Caruso, *Adv. Mater.* 13 (2001) 11.
- [4] (a) L.M. Liz-Marzan, M. Giersig, P. Mulvaney, *Chem. Commun.* (1996) 731;  
(b) L.M. Liz-Marzan, M. Giersig, P. Mulvaney, *Langmuir* 12 (1996) 4329.
- [5] S. Sun, C.B. Murray, D. Weller, L. Folks, A. Moser, *Science* 287 (2000) 1989.
- [6] (a) R.F. Ziolo, E.D. Giannelis, B.A. Weinstein, M.P. Ohoro, B.N. Ganguly, V. Mehrotra, M.W. Russel, D.R. Huffman, *Science* 257 (1992) 219;  
(b) B. Stahl, N.S. Gajbhiye, S. Wilde, D. Kramer, J. Ellrich, M. Ghafari, H. Hahn, H. Gleiter, J. Weißmüller, R. Wurschum, P. Schlossmacher, *Adv. Mater.* 14 (2002) 24.
- [7] (a) M. Giersig, M. Hilgendorff, *J. Phys. D Appl. Phys.* 32 (1999) L111;  
(b) A. Yoshizawa, Y. Nakane, N. Arisawa, H. Imaizumi, H. Sugino, S. Harada, *IEEE Trans. Magn. MAG-23* (1987) 2874.
- [8] (a) X. Xu, G. Friedman, K.D. Humfeld, S.A. Majetich, S.A. Asher, *Chem. Mater.* 14 (2002) 1249;  
(b) S.A. Gomez-Lopera, R.C. Plaza, A.W. Delgado, *J. Colloid Interface Sci.* 240 (2001) 40.
- [9] D. Portet, B. Denizot, E. Rump, J.J. Lejeune, P. Jallot, *J. Colloid Interface Sci.* 238 (2001) 37.
- [10] T. Ung, L.M. Liz-Marzan, P. Mulvaney, *J. Phys. Chem. B* 103 (1999) 6770.
- [11] (a) Y. Lu, Y. Yadong, B.T. Mayers, Y. Xia, *Nano Lett.* 2 (2002) 183;  
(b) C.D. Bain, J. Ewall, G.M. Whitesides, *J. Am. Chem. Soc.* 111 (1989) 7155–7164.
- [12] T. Ji, V.G. Lirtsman, Y. Avny, D. Davidon, *Adv. Mater.* 13 (2001) 1253.
- [13] (a) M. Wu, Y.D. Zhang, S. Hui, T.D. Xiao, S. Ge, W.A. Hines, J.I. Budnick, *J. Appl. Phys.* 92 (2002) 491;  
(b) Y. Kobayashi, M. Horie, M. Konno, B. Rodrigues-Gonzalez, L.M. Liz-Marzan, *J. Phys. Chem. B* 107 (2003) 7420.
- [14] G. Viau, F. Fievet-Vincent, F. Fievet, *J. Mater. Chem.* 6 (1996) 1047.
- [15] (a) C. Xu, K. Xu, H. Gu, X. Zhong, Z. Guo, R. Zheng, X. Zhang, B. Xu, *J. Am. Chem. Soc.* 126 (2004) 3392–3393;  
(b) H. Gu, X. Zhang, B. Xu, *J. Am. Chem. Soc.* 126 (2004) 5664–5665.
- [16] N. Shukla, C. Liu, P.M. Jones, D. Weller, *J. Magn. Magn. Mater.* 266 (1–2) (2003) 178–184.
- [17] J. Garcia-Otero, M. Porto, J. Rivas, A. Bunde, *Phys. Rev. Lett.* 84 (1) (2000) 167–170.